Journal of Manufacturing Processes 57 (2020) 233–243

Contents lists available at ScienceDirect

Journal of Manufacturing Processes

journal homepage: www.elsevier.com/locate/manpro

Hybrid numerical modeling of Friction Assisted Joining

F. Lambiase*, A. Di Ilio, A. Paoletti

Dept. of Industrial and Information Engineering and Economics, University of L'Aquila, via G. Gronchi 18, Zona Industriale di Pile, 67100, AQ, Italy

ARTICLE INFO

Keywords:
Process modeling
Finite element
Hybrid structures
Hybrid joints
Hybrid modeling

ABSTRACT

A hybrid non-linear numerical model of the thermal field produced during Friction Assisted Joining process of Metal-polymers hybrid joints is developed. The model uses experimental processing loads (plunging load and torque) measured during an experimental campaign as inputs. A hybrid approach was used to simulate the contact between the tool and the metal sheet. Indeed, the plunging load was simulated as a prescribed load acting on the punch while the friction heat owing to the interaction of the rotating tool with the metal sheet was simulated as a distributed heat flux over the tool-metal contact surface. This enabled a dramatic reduction of the complexity of the model along with a short simulation runtime. During experimental tests, an IR camera was used to measure the real temperature evolution. These data were used to calibrate and validate the FE model. The results indicated that the developed model can accurately predict the temperature field on the upper metal surface. Thus, it can be readily used to forecast the temperature evolution and distribution and the metal-polymer interface, which is the most influencing factor that determines the mechanical behavior of this type of joints.

1. Introduction

Hybrid multi-materials structures are rapidly spreading in several production fields for structural parts including automotive, aeronautics, electronics, etc. This is due to the possibility to use proper material at the right place. The production of hybrid structures requires the coupling of parts made of extremely different materials, such as metals, polymers, composites. This is generally achieved by mechanical fastening processes as well as adhesive bonding. The severe limitations and drawbacks of these processes demand new solutions. Thermomechanical joining processes, such as ultrasonic joining [1–3], friction lap joining [4–7], laser assisted joining [8–12], friction spot joining [13–15], injection molding [16,17], friction riveting [18–20] etc. meet this demand. In all these processes, the metal-polymer (or composite with thermoplastic matrix) interface is heated by means of different mechanism. Then, an external pressure is applied leading to the formation of the joint. This is due to different mechanisms including chemical bonding [21], physical bonding and development of micro-mechanical fastening. Therefore, the joining mechanism is triggered by the achievement of a certain temperature (mainly dependent on the polymer characteristics) and the applied pressure (which is generally less relevant). The quality of these joints is then highly influenced by the temperature distribution and evolution at the metal-polymer interface. However, direct measurements are very complex. Indeed, InfraRed IR systems do not permit to measure the temperature of hidden surfaces (at the metal-polymer interface), while other measurement sensors such as thermocouples and thermistors are characterized by several issues (relatively long delay time, difficulty to be placed at the interface, etc.). In addition, thermocouples and thermistors provide only spot information; then, they are not able to capture the temperature difference that characterize the metal-polymer interface during the joining processes.

Numerical models have been developed for laser assisted direct joining of metal-polymer components. Here, the laser-material interaction is generally modelled throughout a distribute heat flux. The heat flux H_f is calculated as: $H_f = \alpha \times P/A$, where α is the coefficient of absorption, P is the power and A is the area of the laser spot. Lambiase et al. [22] developed a robust procedure for calibration and validation of FE models used for the prediction of the thermal field. Based on this model, the authors established a relationship between the temperature field at the metal-polymer interface and the shear load of the joints [11] and determined the main factors influencing the temperature distribution [23]. However, while in laser processes the power is an explicit input of the model, in other processes such as Friction Assisted Joining, the frictional power changes over time. Indeed, the power depends linearly by the tool rotation speed and by the torque. The torque, in turn changes over time during the joining process as the temperature of the material in contact with the tool significantly affects

* Corresponding author at: Monteluco di Roio, 67040, AQ, Italy.
E-mail address: francesco.lambiase@univaq.it (F. Lambiase).

https://doi.org/10.1016/j.jmapro.2020.06.031
Received 6 May 2020; Received in revised form 17 June 2020; Accepted 22 June 2020

the yield and shear stress. Finally, the friction coefficient is also function of the temperature.

Because of the great difficulties to measure the temperature distribution at the metal-polymer interface, the common practice has been to refer to the temperature of the upper metal surface [24,25]. This enabled to understand the influence of the process conditions (such as plunging load, dwell time, clamping frame material) on the temperature qualitatively. In addition, some relationship between the temperature and mechanical characteristics of the joints were established in [26,27]. However, the above studies involved low power equipment that required relatively long dwell time (up to 30 s) to produce activate the joining mechanism. More recently, the development of a new instrumented machine characterized by higher power and load capacity, enabled the reduction of the joining time to 2 s per joint.

The present paper introduces a hybrid experimental-simulation approach based on the adoption of experimental data of the plunging load and torque measured during Friction Assisted Joining of metal-polymer sheets. These data are then used as input into a Finite Element model, where the frictional heat is introduced as a variable heat flux over the contact tool-metal interface. Experimental tests were conducted on Aluminum alloy AA7075 and polyamide PA66 sheets. The tests were performed under different processing conditions (by varying the plunging loading and the tool rotation speed). The model was calibrated and validated by comparing the experimental measurements of the temperature field during the process (by means of an IR camera) on the visible surfaces and the temperature maps predicted by the numerical model.

2. Materials and methods

2.1. Hybrid approach

Friction assisted joining process involves a rotating tool that is forced with a prescribed plunging load against the sheets being coupled. This phase is generally conducted for a prescribed Dwell time, then the tool is rapidly retracted, and the joint consolidates (cools down). During the production of metal-polymer joints the metal sheet is placed in contact with the tool. The frictional heat produced at the tool metal interface is rapidly conducted towards the metal-polymer interface. Here, the heat accumulates since the poor thermal conductivity of the polymer. Therefore, the joint between the metal and the sheet is triggered as a certain temperature (close to the melting temperature of the polymer) is reached. From a simulation point of view, the interaction between the tool rotating at high speed and the metal involves several issues [28–30]. These include:

1 Severe distortion of the mesh of the metal in correspondence of the contact region with the tool [31,32], owing to high temperature of the metal and significant loss of bearing load capacity (and shear stress);
2 High contact non-linearity owing to high speed tool rotation (which would benefit of explicit time integration);
3 Steep temperature differences (especially for processing conditions involving high power) which would require small element (that affect the efficiency of explicit time integration);
4 Significant variation of friction conditions at the tool metal interface [33];
5 All the above issues determine extremely long simulation time.

In addition, modeling heat generation at the tool-metal interface would also involve complex modeling [34–37]. On the other hand, a hybrid approach based on a close integration between experimental measurements and numerical model, would enable to overcome all the above-mentioned issues, enabling the possibility to achieve accurate predictions of the temperature at the metal-polymer interface in extremely low simulation time. Thus, if the frictional power in known (for example by monitoring the torque during the process), this can be simulated as a distributed heat flux acting over the tool-metal interface. This approach was followed in the present work.

2.2. Experimental details

Friction Assisted Joining experiments were performed on AA7075 aluminum alloy and polyamide PA66 plates. The samples were 3 mm and 5 mm thick, respectively. Metal and polymer samples (25 mm wide and 80 mm long) were cut from unique sheets. The overlapping area was 25 × 25 mm^2.

Experimental tests were conducted by using a prototypal CNC machine. This involved a Universal testing machine model 322.31 by MTS and a high-power spindle with maximum power of 13.5 kW and maximum rotation speed of 8000 RPM. The tests were performed under load control by imposing the plunging load curve and tool rotation speed. Processing loads: plunging and torque were measured during the process by means of two piezo-electric cells, model 9055-9063B by Kistler. The signals from the cells were conditioned by means of a multichannel charge amplifier model 5017 by Kistler and then acquired by means of an I/O acquisition board model USB6009 by National Instrument at a sample rate of 2.0 kHz. The temperature variation during the process was measured by means of an IR cameral model E60 by Flir, at a sample rate of 30 Hz. The camera was placed at almost 300 mm from the contact region between the tool and the aluminum sheet, at an angle of incidence of 60 deg. Because of the high reflectivity of the aluminum sheet, the aluminum sample was covered by a thin graphite layer. This enabled to increase the surface emissivity to almost 0.80. The emissivity was determined using the procedure reported in [22]. During the experiments, the tool was plunged against the metal sheet, which was placed over the polymer sample. The tool was made of a high strength steel K720 by Bohler. The tool had a cylindrical geometry with a diameter of 10 mm and corner radius of 0.1 mm. A schematic of the experimental setup is depicted in Fig. 1.

An experimental campaign of friction assisted joining tests were conducted by varying the main processing conditions, including: the tool rotation speed (ω), the plunging load (F_p) and the dwell time (D_t). The lowest and highest levels for each processing condition are reported in Table 1.

2.3. Numerical model

A thermo-mechanical model of the friction Assisted Joining process was developed based on a non-linear finite element (FE) modeling. Implicit time integration was involved within Abaqus 6.17 environment. The adoption of the implicit solver was driven by the necessity of using different mesh densities efficiently. An explicit time integration would require localized mass scaling based on the different dimension of the elements. For a coupled thermo-mechanical analysis, this could not be handled automatically by Abaqus as automatic mass scaling does not modify the heat capacity element-by-element. In addition, the tool

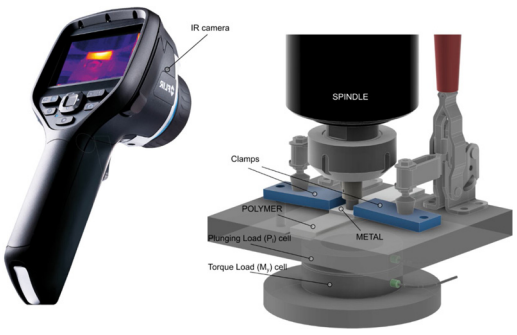

Fig. 1. Schematic of the equipment used to produce FAJ joints.

Table 1
Range of levels of the process conditions involved in the experimental campaign.

Level	Tool rotation speed, (ω) [RPM]	Plunging Load, (F_p) – [N]	Dwell time, (Dt) – [s]
Lowest value	2000	100	2
Highest value	8000	600	15

rotation is not simulated but rather the frictional heat is simulated as a heat flux. Thus, low nonlinearity of contact conditions and moderate localized deformation of the aluminum sheet under the tool can be easily handled by the implicit solver.

The aluminum and the polymer samples were simulated as deformable components, by means of linear 8-nodes brick elements. The tool was simulated as a rigid component with nodal temperature degree of freedom. The tool was fully constrained, with exception for the motion along the plunging direction (Y direction). On the other hand, a prescribed plunge load curve $P_l(t)$ (derived from experimental measurements) was applied along the Y direction, as schematized in Fig. 3. An YZ-plane of symmetry was used to reduce the number of involved elements. The tool-metal interaction was simulated by surface-to-surface contact algorithm with thermal conductance. The thermal conductance coefficient was set to 6000 W m^{-2} K^{-1} [38]. A sensitivity analysis was performed on this parameter and the results showed that above 1000 W m^{-2} K^{-1} the thermal conductance showed negligible influence on the temperature distribution. On the other hand, the metal-polymer parts were simulated as a unique part (sharing the nodes at the interface).

On the other hand, the frictional heat was simulated as a surface heat flux over the tool-metal interface region. A similar approach has been already used for friction welding [39,40] and enabled a very effective calculation of the temperature and material flow. As the frictional heat depends on the relative velocity between the contact surfaces, a linear heat flux distribution was used, as schematized in Fig. 2.

The frictional power supplied to the metal is calculated as:

$$P(t) = M_y(t) \bullet \omega \tag{1}$$

where $P(t)$ is the instant power depending on the torque $M_y(t)$ and ω the rotation speed. Since the heat flux is supposed to increase linearly with the distance from the tool axes (r), thus $H_f = m \bullet r$. Therefore, the heat flux H_f distribution was calculated by imposing that the integral of the distribution equals $P(t)$.

$$P(t) = \int_0^{2\pi} \int_0^{D/2} H_f \, dr d\theta = \int_0^{2\pi} \int_0^{D/2} m \bullet r dr d\theta \pi = \frac{2}{3} \pi m \left(\frac{D}{2}\right)^3 \tag{2}$$

where m is the unknown slope of the linear heat flux distribution. Thus, m is given by Eq. (3):

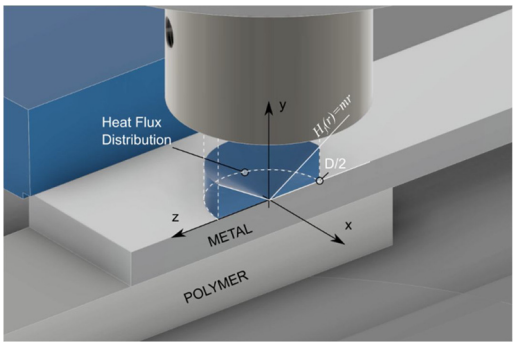

Fig. 2. Schematic of heat flux distribution.

$$m = \frac{3}{2\pi} \bullet \frac{P(t)}{\left(D/2\right)^3} = \frac{3}{2\pi} \bullet \frac{\omega}{\left(D/2\right)^3} \bullet M_y(t) \tag{3}$$

$$\delta = \frac{3}{2\pi} \bullet \frac{\omega}{\left(D/2\right)^3} \tag{4}$$

$$m = \delta \bullet M_y(t) \tag{5}$$

if δ is the magnitude (constant), the frictional power, simulated as a heat flux distribution, is given by Eq. (6):

$$H_f = \delta \bullet M_y(t) \bullet \sqrt{X^2 + Z^2} \tag{6}$$

Fourier's heat transfer equation Eq. (7) was adopted to solve the thermal field during the heating step.

$$\frac{\partial}{\partial x}\left(k\frac{\partial T}{\partial x}\right) + \frac{\partial}{\partial y}\left(k\frac{\partial T}{\partial y}\right) + \frac{\partial}{\partial z}\left(k\frac{\partial T}{\partial z}\right) = \rho c_p \frac{\partial T}{\partial t} \tag{7}$$

The model involved convection heat loss (q_c), which was calculated by Eq. (2):

$$q_c = h(T_s - T_0) \tag{8}$$

where h = 15 W/(m^2·K), such a value is widely used in similar simulations [23].

Radiation towards surrounding environment was also involved in the simulation by using the Stefan–Boltzmann law, as described by Eq. (9):

$$P = e \bullet \gamma \bullet A_{sur} \bullet (T^4 - T_e^4) \tag{9}$$

Where, e is the surface emissivity (0.8), γ is the Stefan-Boltzmann constant (5.670374419 × 10^{-8} W·m^{-2}·K^{-4}), T is the average element temperature, T_e is the environment temperature (30 °C) and A_{sur} is the surface of the element.

2.4. Materials parameters

A Johnson-Cook model was used to describe the flow stress of the AA7075 material as a function of temperature and strain and strain rate as described by Eq. (10), with the material constants reported in Table 2.

$$\bar{\sigma} = (A + B\varepsilon_p^n)\left[1 + C ln\left(\frac{\dot{\varepsilon}}{\dot{\varepsilon}_0}\right)\right](1 - \theta^m) \tag{10}$$

with:

$$T = \begin{cases} 0 & for\ T < T_{transition} \\ (T - T_{transition})/(T_{melt} - T) & for\ T_{transition} \le T \le T_{melt} \\ 1 & for\ T > T_{melt} \end{cases} \tag{10}$$

where, ε_p is the plastic strain, $\frac{\dot{\varepsilon}}{\dot{\varepsilon}_0}$ is the plastic strain rate, A is the yield stress at 0.2 % offset strain, B and n describe strain hardening effects. The materials constants are reported in Table 2.

For the aluminum AA7075, temperature-dependent material parameters were adopted, as shown graphically in Fig. 4 (also reported in table format).

The main physical and mechanical characteristics of the PA66 used in the simulation are reported in Table 3.

3. Results

3.1. Experimental measurements of the processing loads

Fig. 5 depicts the experimental loads acquired during the FAJ process varying the plunging load and the tool rotation speed. The plunging loads, as measured by the external load cell were characterized by a steep increase (1000 N/s) until the prescribed plunging load was

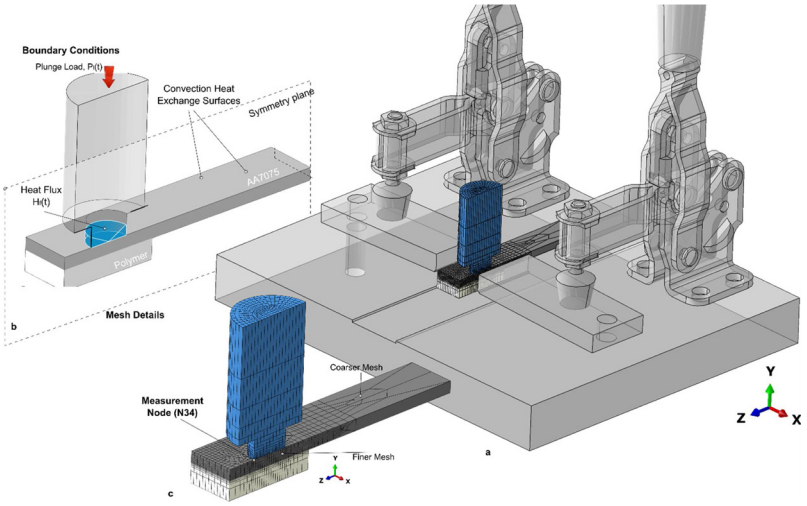

Fig. 3. (a) Schematic of assumed geometry of the experimental setup; (b) Boundary conditions; (c) mesh and (d) closer view of mesh at the interface region, showing the measurement node N34.

Table 2
Material constants (Johnson-Cook model) used for AA7075 [41].

A [MPa]	B [MPa]	C	n	m	Melting Temperature [°C]	Transition Temperature [°C]
546	678	0.024	0.71	1.56	620	20

reached. Please note that some differences between the nominal load and the experimental value are observable. This was due to the adoption of a load cell of 250 kN (with gain of 10 to achieve a full-scale of 25 kN) to perform a closed loop control over a much lower prescribed load (from 100 N to 600 N). As the prescribed plunging load was reached, the load held almost constant. However, compared to the load trends, the torque showed higher variation during the dwell phase, especially under processing conditions involving high tool rotation speed (ω = 6000 RPM and ω = 8000RPM). These owned to the material flow confined at the upper aluminum surface (almost 0.1 depth) that altered the contact conditions between the tool and the metal. This is clearly observable by the imprint left by the tool on the upper metal surface, as shown in Fig. 5c. The complex and shallow material flow developing at the tool-metal interface further increases the difficulty of an analytical model or a pure FE model (where the inputs are the plunging load and the tool rotation speed) to predict the temperature field reached during the process.

As expected, regardless the adopted tool rotation speed and dwell time, higher plunging loads involved higher torque. Indeed, the torque balances the momentum given by the shear force, which is proportional to the normal load (plunging).

3.2. FE model validation

The validation of the numerical model was performed by comparing the temperature predicted in correspondence of the node showed in Fig. 3c with the peak temperature calculated frame by frame by the analysis of the IR maps. The adoption of the max operator over a region of Interest ROI, was driven by several issues, as follows:

- The heated region was relatively small. In addition, the camera was characterized by relatively low resolution (320 × 240 pixel) and positioned at 300 mm from the workpiece. This led to a relatively low number of pixels within the heated region. Consequently, a given point could refer to the edge of the tool and, at the same time to the metal sheet. This may bias the measurements. On the other hand, the adoption of the maximum temperature over the region would be more representative and less affected by such an issue;
- the selection of a given point is more subjective than the calculation of the maximum temperature;
- during the tests, the sample moved with respect to the camera, thus a fixed point of the camera would be not representative of a specific point of the sample;
- inevitable vibrations could further produce small displacements of the sample (and the target point) with respect to the IR camera;
- material expelled during the process (which is characterized by an emissivity that different from that pf the graphite) could “cover” the target point.

Fig. 6 compares the variation of the peak temperature (calculated frame-by-frame) by means of the IR camera with numerical prediction of the temperature at the node in Fig. 3c, for different processing

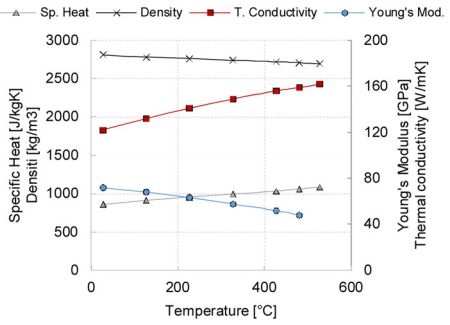

Temp. [°C]	Thermal cond. [W m^{-1}K^{-1}]	Spec. Heat [J Kg^{-1}K^{-1}]	Density [kg m^{-3}]	Young's Modulus [GPa]
30	122	862	2810	71.85
130	132	913	2780	68.1
230	141	955	2760	63
330	149	994	2740	57
430	156	1036	2720	52
480	159	1060	2708	48
530	162	1084	2696	

Fig. 4. Physical and mechanical characteristics of AA7075 [42].

Table 3
Physical and mechanical characteristics of PA66.

Thermal Conductivity [W m^{-1} K^{-1}]	Young's Modulus [MPa]	Compressive Yield Stress MPa]	Specific Heat [J kg^{-1} K^{-1}]	Melting Temp. [°C]	Thermal Exp. (CLTE) [K^{-1}]	Density[kg m^{-3}]
0.36	3500	85	1500	258	10^{-5}	1150

conditions. The comparison indicates that there is a good agreement between the FE model predictions and experimental measurements. This is true even in those tests characterized by significant variability of the torque during the process (at high tool rotation speed ω = 6000 RPM and ω = 8000 RPM). The good accuracy of the model can be also appreciated by the replication of the features concerning the temperature-time trends.

3.3. Analysis of metal-polymer interface temperature

The strength of metal-polymer joints is mostly determined by the temperature distribution at the metal-polymer interface. In this region, the temperature should be high enough to allow the polymer to properly soften/melt, and at the same time avoid adverse phenomena such as cavity formation, and polymer degradation. Fig. 7 depicts the temperature maps of the upper metal surface and the cross-section of the metal and polymer components during FAJ. After a heating time of t = 0.5 s (please note that in Fig. 7a the peak temperature of the colormap is set to 150 °C), the upper surface is suddenly heated and the heated region is localized in correspondence of the tool edge. This is more evident from the cross-section temperature map that shows a "camel humps" distribution. As the heat is supplied by the friction generated at the tool-metal interface, temperature decreases as moving from the upper metal surface towards lower layer of the metal sheet. On the other hand, the polymer is heated only in correspondence of a thin layer under the interface owing to its lower thermal diffusivity. For relatively short heating time (t = 0.5 s), steep temperature difference exists between the upper metal surface and the metal-polymer interface. As the process proceeds, the longer interaction time, the high thermal diffusivity of the aluminum and the poor thermal diffusivity of the polymer, tend to reduce the temperature difference between the upper surface of the metal sheet and the metal-polymer surface, as depicted in Fig. 7b–f. This involves a lower temperature rise as the frictional heat is rapidly spread towards surrounding and underlying regions. As the cooling phase starts and the tool is retracted from the joint, the temperature rapidly decreases as heat conduction diffuses heat towards the surrounding regions.

To better comprehend the evolution of the temperature during the process, reference nodes in correspondence of the tool axis and tool edge at the upper surface of the metal sheet and at the metal-polymer interface were analyzed. Fig. 8a and b indicate the position of these reference nodes. The temperature history is reported for a reference case (ω = 8000 RPM and F_p = 600 N), as depicted in Fig. 8c. At the beginning of the process, the temperature increases more rapidly in correspondence on the tool edge (N34) as compared to the tool axis (N403) because of the higher tool rotation speed (as it is also indicated by the temperature map shown in Fig. 7a). After 0.5 s, this trend is reversed and the temperature in correspondence of the tool edge axis

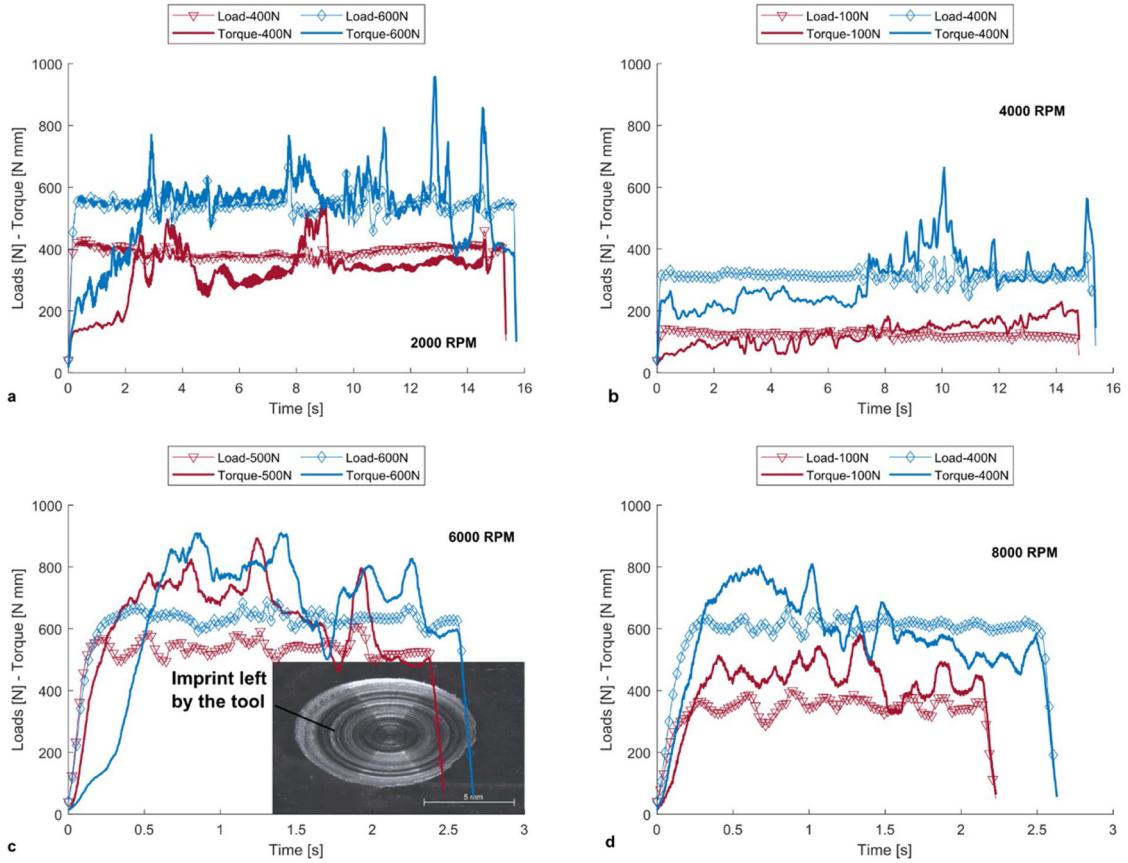

Fig. 5. Experiemntal measurements of the plunging load and torque measured during the process at different processing conditions (plunging load, tool rotation speed and dwell time).

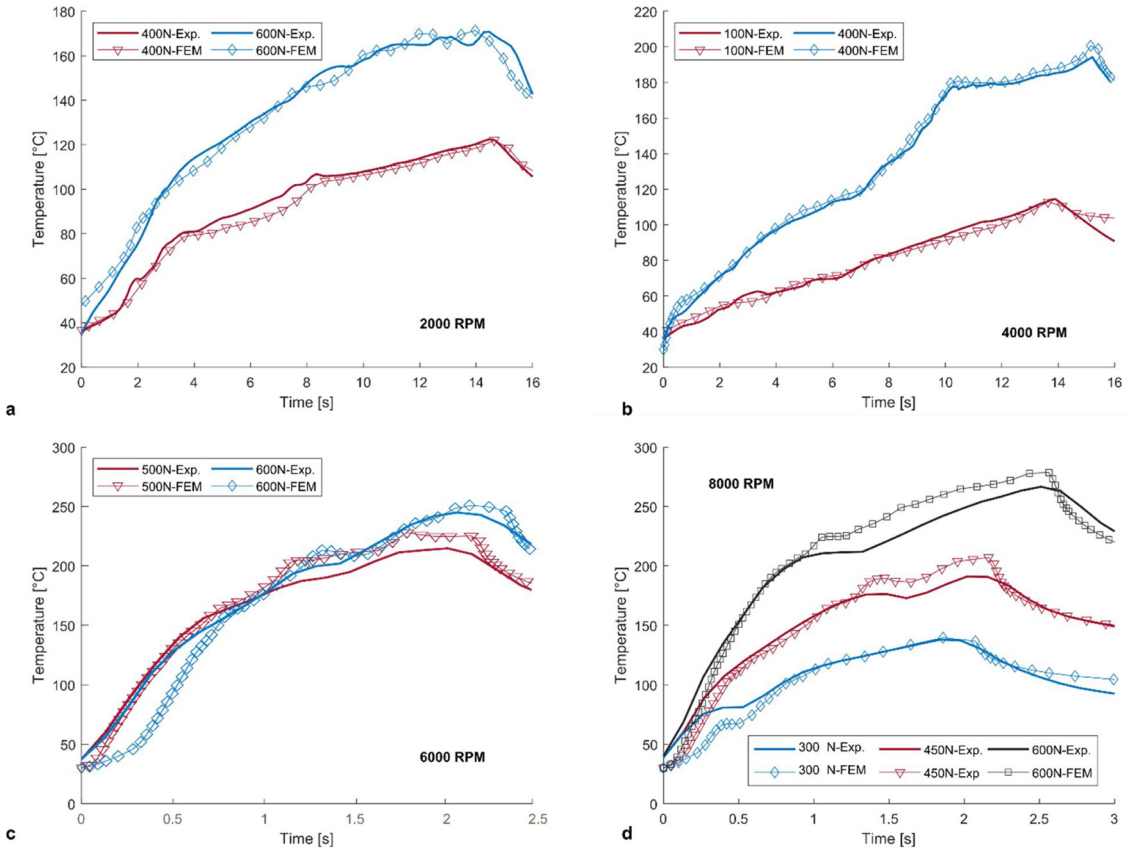

Fig. 6. Comparison of experimental measurements of the temperature (using max operator) and numerical prediction of the temperature at the node N34 under different processing conditions.

increases more slowly than that at the tool axis. This owns to the higher heat loss from the node (N34) towards surrounding regions.

The temperature difference between the upper metal surface and the metal-polymer interface is monitored throughout the temperature differences between the nodes N403-N363 (center) and the nodes N34-N18 (edge), as reported in Fig. 8d. The temperature difference between the upper and lower surface is more pronounced at the edge as compared to the center. In addition, it is highly influenced by the processing time. Indeed, at the beginning, the difference increases very steeply. As an example, after 0.7 s the temperature difference in correspondence of

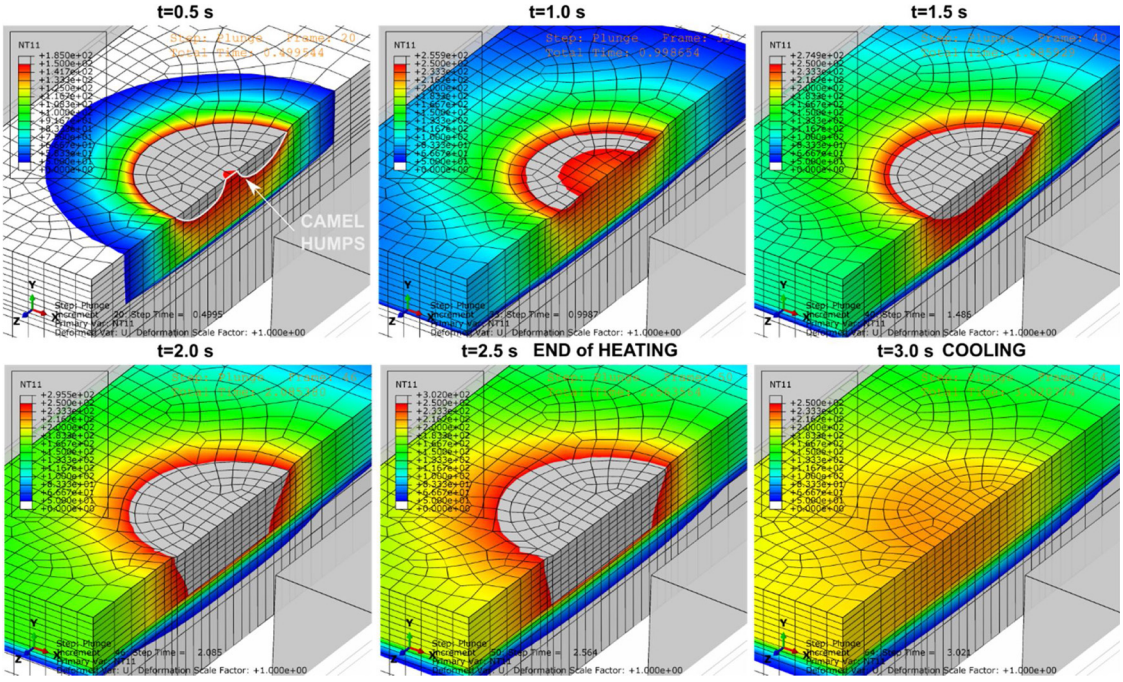

Fig. 7. Evolution of temperature during FAJ process (ω = 8000 RPM, F_p = 600 N).

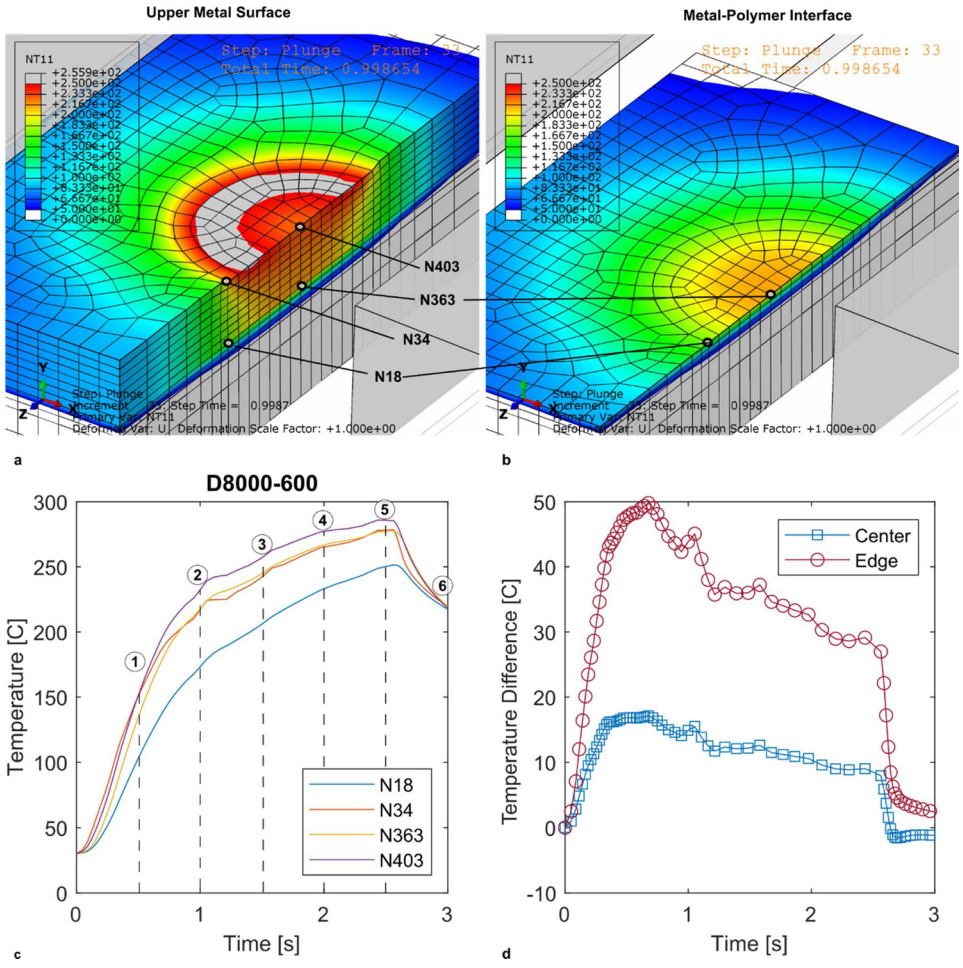

Fig. 8. Variation of temperature difference between upper metal surafce and metal-polymer interface during the process, (ω = 8000 RPM, F_p = 600 N).

the edge rises to 50 °C. However, as the process proceeds, the temperature difference reduces because of different mechanisms. At the top surface, the increase of the temperature comes with higher heat loss by heat conduction, radiation and convection. In addition, the longer interaction time also comes with higher amount of heat conducted towards the metal-polymer interface, which also contributes to reduce the temperature difference during the process. At the end of the dwell time, the difference reduces almost immediately (after 0.5 s from the end of the dwell time).

The above results indicate that the temperature at the metal-polymer interface can be very different to that observed on the metal surface (observable for example by the IR camera). Thus, the prediction of the mechanical behavior of the joints based on the temperature measured on the upper metal surface would be unreliable. In addition, the trends reported in Fig. 8d indicate that the temperature difference changes during the processing time.

The temperature distribution on the upper metal surface and at the metal-polymer interface is characterized by three areas: 'region 1' under the tool (which is characterized by the highest temperature), 'region 2' the area close to the metal edge and 'region 3' which is the opposite region, as depicted in Fig. 9. These last two regions are characterized by different temperatures. In region 2 heat accumulates near the metal edge, which transfers heat only to the environment. Thus, the temperature in the region 3 is lower as the heat is also transferred to the rest of the metal sheet.

The temperature predicted by the FE model highlighted significant insights into the characteristics of the temperature distribution during the process. First, it enabled to retrieve information about hidden regions, such as the metal-polymer interface and the region of the upper

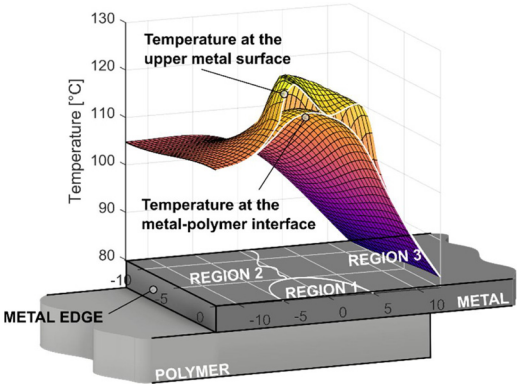

Fig. 9. Temperature distribution at the upper metal surface and metal-polymer interface, (ω = 2000 RPM, F_p = 400 N).

metal sheet that is in contact with the tool. As depicted in Fig. 10a, d and g, the region under the tool (which is highlighted with a transparent grey cylinder) is that characterized by the peak temperature T_p. On the other hand, depending on the processing conditions involved, the maximum temperature directly observable T_o (surrounding the tool-metal interface area) can be much lower than T_p. For instance, for conditions reported in Fig. 10d, T_p = 225 °C and T_o = 160 °C, this would lead to an underestimation of the peak temperature of 65 °C. Obviously, such a difference depends on the processing conditions involved (and the thermal diffusivity of the metal sheet). This difference increases with the involved power and decreases with the dwell time, as

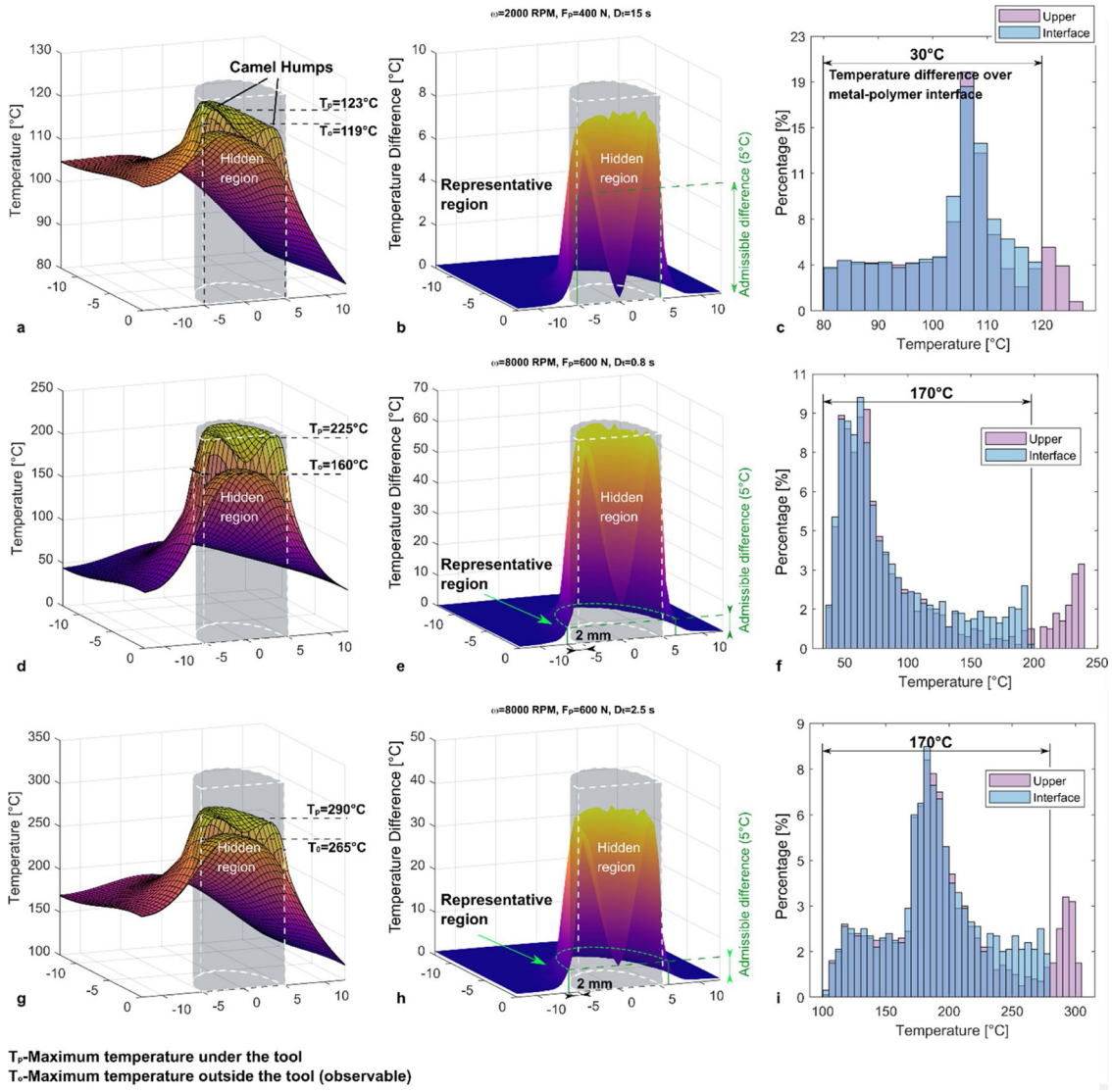

Fig. 10. Temperature distribution at the upper surface of the metal sheet and metal-polymer interface for different processing conditions.

can be observed by comparing the maps of Fig. 10a with those of Fig. 10d.

The distribution of the temperature difference between the upper metal surface and the metal-polymer interface is reported in Fig. 10b. The temperature difference surface indicates that the higher difference concentrates near the tool edge (where higher power is generated by friction); while, the much lower differences were found in regions surrounding the tool. Supposing that 5 °C could be considered an admissible difference, Fig. 10b indicates that the entire region surrounding the tool is representative; while for processing conditions involving higher power (as those depicted in Fig. 10e and h), only a small portion (at a distance of 2 mm from the tool edge) of the visible area is characterized by a temperature difference higher than 5 °C. The above results indicate that, the temperature of the upper metal surface is indicative of the temperature at the metal-polymer interface for the overlapping area except for the area under the tool and eventually, a restricted region surrounding the tool edge.

The histogram plots in Fig. 10c, f, and i provide further insight into the features of the temperature distribution. Indeed, they quantify the isothermal areas after a given interaction time as a percentage of the entire metal-polymer interaction area. First, the temperature difference over the metal-polymer interface region depends on the power supplied, while it appears to be negligibly influenced by the dwell time (as can be inferred by comparing Fig. 10f, and i). Conditions involving low power levels (such as $\omega = 2000$ RPM and $F_p = 400$ N) led to a homogeneous distribution of temperature (almost 30 °C). This was also caused by the prolonged dwell time that facilitates the frictional heat to be spread over the surrounding regions. On the other hand, processing conditions involving much higher power ($\omega = 8000$ RPM and $F_p = 600$ N), involved higher temperature difference at the metal-polymer interface (almost 170 °C).

Fig. 11 cross the temperature difference with the frictional power calculated as the product of the torque by the tool rotation speed under different processing conditions. The temperature difference between the upper metal surface and the metal-polymer interface follows the variation of the power during the process. In addition, processing conditions involving higher amount of power (e.g. higher amount of tool rotation speed and/or higher plunging loads) come with steeper temperature differences. For example, for $\omega = 2000$ RPM and $F_p = 400$ N the process involved a power up to 150 W and a peak difference up to 7 °C, while for $\omega = 8000$ and $F_p = 600$ N the process involved a power up to 900 W and a peak temperature difference up to 50 °C. These trends were expectable since higher amount of power would involve higher heating rate and consequently higher difference between the temperature of the directly heated region (surface in contact with the tool) and the surrounding and underlying regions.

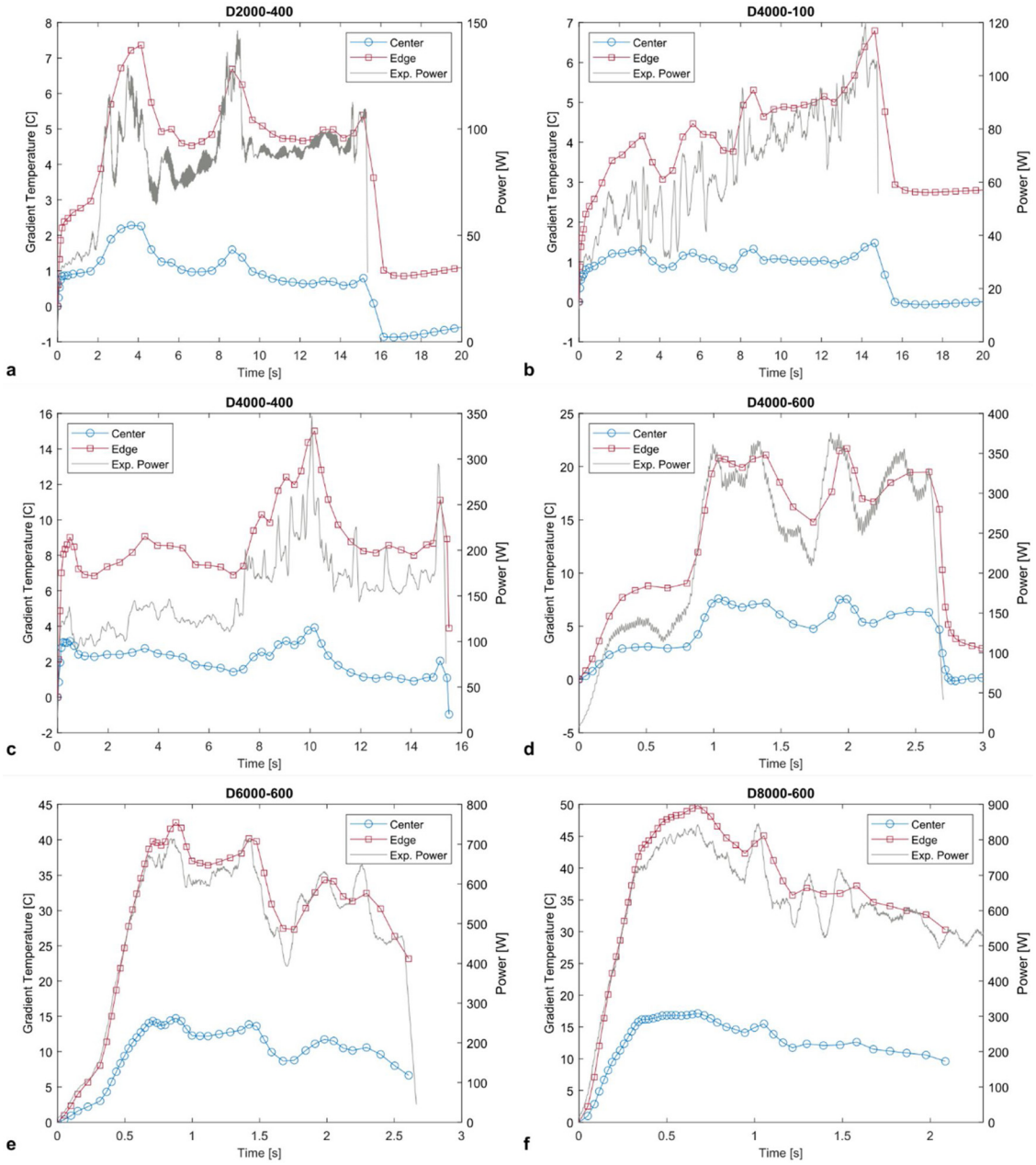

Fig. 11. Temperature difference (between top metal and metal-polymer interface) at cented and edge positions simulated by the FE model under different processing conditions.

The correlation between the power supplied and the temperature difference measured at the edge of the tool (and the corresponding node at the metal-polymer interface), is graphically reported in Fig. 12. The plot indicates the apparent increase of the temperature difference with the frictional power during the process. In addition, even if small oscillation of the temperature difference around the linear fitting curve, the frictional power appears to be the most influencing parameter of the temperature difference.

4. Discussion

Friction Assisted Joining represents a promising process for production of hybrid metal-polymer structures. It has been used for high strength and lightweight materials such as aluminum and titanium alloys coupled with different tecnopolymers (including PEEK and PA). The results from previous researches identified the potential advantages of FAJ process such as simplicity, possibility of automation, low processing time and high mechanical strength of the joints.

Previous researches about similar processes, such as Laser Direct Joining, have determined the relationship between the maximum shear force of the joints and the temperature reached at the metal-polymer interface during the process. The joining mechanism is triggered by the achievement of a threshold temperature. However, direct measurements of the interface are very complex to be performed. On the other hand, temperature measurements at the upper metal surface, which is in contact with the tool, can be easily performed by means of IR equipment such as an IR camera. Nevertheless, the prediction of the joint strength as well as the joined area dimension based on the solely measurement of the upper metal surface may lead to inaccurate results. Furthermore, despite of laser direct joining, during Friction assisted joining the upper metal surface is not entirely visible (as it is covered by the tool, consequently the temperature in that region is unknown. These considerations highlighted the need of a predictive tool capable to analyze the temperature history and distribution during friction

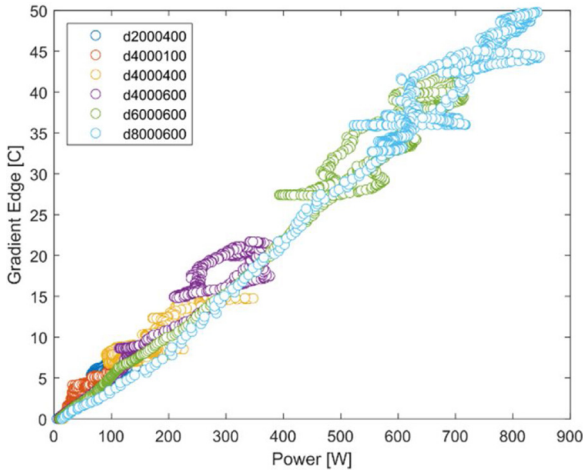

Fig. 12. Correlation between Power and temperature difference in correspondence of the tool edge between upper and lower metal surface.

assisted joining process.

The numerical model developed and validated in this paper meets this demand. The model uses real data such as absorbed power measured during the process and simulates the frictional heat produced by the interaction of the tool with the metal sheet as a distributed heat flux. The comparison between IR measurements acquired on the upper metal surface and the predictions of the FE model indicated the reliability of the model under several and very different process conditions.

The results indicated that, the peak temperature region lies in the tool-metal contact region; therefore, it cannot be measured by experimental equipment. In addition, depending on the processing condition, the temperature under the tool can be much higher than visible regions (surrounding the tool). When processing conditions involving high power amounts (600 W), this difference reached 65 °C. The results from the model simulations also clarified the influence of the process conditions on the temperature difference between the upper metal surface (which can be generally observed by means of IR cameras) and the metal-polymer interface (which influences the joint characteristics such as the extension of the joined area and the strength). The temperature difference decreases with the tool-metal interaction time and increases with the frictional power. This indicates that, when processing conditions involving low power are used, which generally require longer dwell time, smooth temperature differences exist between the upper and lower surface. Thus, the temperature of the upper metal surface is highly indicative of that developing at the metal polymer interface. On the other hand, when high power is used, which generally comes very short heating time, the temperature of the upper surface can be even 70 °C higher than that at the metal-polymer interface. Thus, the extension of the joined area based on the temperature reached at the upper metal surface would be highly overestimated. It is worth noting that this analysis was performed on a highly conductive material (the thermal conductivity of AA7075 is 130 W m^{-1} K^{-1}). Thus, steeper temperature differences would be expected when titanium alloys (with a thermal conductivity of about 22 W m^{-1} K^{-1}) and steel alloys (with a thermal conductivity ranging between $10-50$ W m^{-1} K^{-1}) would be used instead on aluminum alloys. In these cases, the adoption of a predictive model appears indispensable.

The great advantage of the developed model consists into the processing of real power data coming from experimental tests. Thus, the temperature forecasts refer to a well-defined history of a specific processing case. This also simplifies the model development and calibration as the obvious variability of the friction conditions with temperature is intrinsically embedded into power data and does not need to be measured or calibrated. In addition, from a simulation point of view, it is more computationally efficient as the severe contact non-linearity between the tool and the metal sheet is not computed. This enabled to perform a simulation in almost 7 min with a workstation equipped with dual Intel Xeon E5-2687W using 4 cores. This simulation time could be reduced by further optimizing the mesh distribution; however, even halving the simulation time, it would not allow a real-time simulation of a joining process while it is conducted. This probably represents the main limit of the developed model that restricts the scope of use for analysis of the influence of the processing conditions and material characteristics on temperature at the metal-polymer interface.

The next step would be the integration of the developed model with an expert system of an Artificial Neural Network. This would enable to train the Network and subsequently use its high computational efficiency for the real-time temperature prediction. Once calibrated and validated such a system could avoid the adoption of the IR camera during the process.

5. Conclusions

A nonlinear FE model of Friction Assisted joining process has been developed with the aim of predicting the temperature distribution and history during the process. The model was validated by comparing the model forecasts with the temperature measurements performed by an IR camera on the upper metal surface. Validation tests were performed by using an instrumented equipment under several processing conditions. The main results of the study are summarized as follows:

- The developed model is capable to predict the temperature at the metal-polymer interface, which represents the key factor influencing the mechanical behavior of the joints. This represents a great improvement with respect to conventional monitoring system based on the experimental measurement of upper metal surface, since the impossibility of such equipment (e.g. the adoption of IR cameras) to determine the temperature under the tool and at the polymer-metal interface;
- The model provides accurate prediction of the temperature at the upper metal surface even in those cases characterized by severe variations/oscillations of the absorbed power during the joining time. The average error was almost 5%. In addition, the adoption of a surface heat flux to model the frictional heat extremely reduced the high contact non-linearities between the tool and the metal sheet, leading to relatively short simulation time (up to 7 min);
- The results indicated that the peak temperature lies under the tool-metal contact area, regardless the process conditions adopted. Thus, the measurement of the upper surface of the metal sheet may lead to severe underestimation of the peak temperature (up to 65 °C). Such a difference increased when processing conditions involving high power amounts were adopted, and reduced with longer dwell time;
- The temperature maps highlighted the presence of three main regions at the metal-polymer interface: (1) the region corresponding to the tool-metal contact area, which is characterized by the highest temperature; (2) the region close to the metal edge which exhibits intermediate temperatures and; (3) the opposite region where the temperature is much lower owing to heat diffusion towards the rest of the metal sheet;
- in the region surrounding the tool, the temperature difference between upper metal surface and polymer-metal interface was negligible, regardless the processing conditions (power, dwell time, tool rotation speed and plunging load). This indicates that in this region, the temperature measured on the upper metal surface would be highly indicative of the corresponding area at the metal-polymer interface;
- in the region underlying the tool, a high temperature difference between the upper metal surface and the metal-polymer interface was observed. This temperature difference was also a function of the processing conditions involved;
- processing conditions involving low power, enabled to homogenize

the temperature at the metal-polymer interface at the expenses of the peak temperature (that was relatively low) even after long dwell time (e.g. Dwell time of 15 s). Thus, low power conditions can be used preferably on polymers characterized by low melting/softening temperature.

- Processing conditions involving high power levels, involved steep temperature differences between the region under the tool and surrounding ones. Under such conditions, the dimension of the joined area is restricted by the tool dimension as the highly localized heating. High power process conditions can be used either for polymers with higher melting/softening temperatures. In addition, as the reduced processing time, heat diffusion is restricted leading to greater energy efficiency;

Author agreement

The article is the authors' original work, hasn't received prior publication and isn't under consideration for publication elsewhere.

Declaration of Competing Interest

The authors declare that they have no known competing financial interests or personal relationships that could have appeared to influence the work reported in this paper.

References

[1] Yeh R-Y, Hsu R-Q. Development of ultrasonic direct joining of thermoplastic to laser structured metal. Int J Adhes Adhes 2016;65:28–32.
[2] Lionetto F, Balle F, Maffezzoli A. Hybrid ultrasonic spot welding of aluminum to carbon fiber reinforced epoxy composites. J Mater Process Technol 2017;247:289–95.
[3] Lionetto F, Mele C, Leo P, D'Ostuni S, Balle F, Maffezzoli A. Ultrasonic spot welding of carbon fiber reinforced epoxy composites to aluminum: mechanical and electrochemical characterization. Compos Part B Eng 2018;144:134–42.
[4] Nagatsuka K, Yoshida S, Tsuchiya A, Nakata K. Direct joining of carbon-fiber–reinforced plastic to an aluminum alloy using friction lap joining. Compos Part B Eng 2015;73:82–8.
[5] Okada T, Uchida S, Nakata K. Direct joining of aluminum alloy and plastic sheets by friction lap processing. Mater Sci Forum 2014;794–796:395–400.
[6] Wirth FX, Zaeh MF, Krutzlinger M, Silvanus J. Analysis of the bonding behavior and joining mechanism during friction press joining of aluminum alloys with thermoplastics. Procedia CIRP 2014;18:215–20.
[7] Liu FC, Liao J, Nakata K. Joining of metal to plastic using friction lap welding. Mater Des 2014;54:236–44.
[8] Jiao J, Jia S, Xu Z, Ye Y, Sheng L, Zhang W. Laser direct joining of CFRTP and aluminium alloy with a hybrid surface pre-treating method. Compos Part B Eng 2019;173:106911.
[9] Li P, Li J, Tan W, Liu H, Wang X. Experimental study on the laser transmission joining of polystyrene and titanium. Materials (Basel) 2018;11(9).
[10] Genna S, Lambiase F, Leone C. Effect of laser cleaning in laser assisted joining of CFRP and PC sheets. Compos Part B Eng 2018;145:206–14.
[11] Lambiase F, Genna S, Kant R. Optimization of laser-assisted joining through an integrated experimental-simulation approach. Int J Adv Manuf Technol 2018.
[12] Lambiase F, Genna S. Laser assisted joining of AA5053 aluminum alloy with polyvinyl chloride (PVC). Opt Laser Technol 2018;107:80–8.
[13] Esteves JV, Goushegir SM, dos Santos JF, Canto LB, Hage E, Amancio-Filho ST. Friction spot joining of aluminum AA6181-T4 and carbon fiber-reinforced poly (phenylene sulfide): effects of process parameters on the microstructure and mechanical strength. Mater Des 2015;66:437–45.
[14] Goushegir SM, dos Santos JF, Amancio-Filho ST. Influence of process parameters on mechanical performance and bonding area of AA2024/carbon-fiber-reinforced poly (phenylene sulfide) friction spot single lap joints. Mater Des 2015;83:431–42.
[15] Yusof F, Muhamad M, Moshwan R, Jamaludin M, Miyashita Y. Effect of Surface States on joining mechanisms and mechanical properties of aluminum alloy (A5052) and polyethylene terephthalate (PET) by dissimilar friction spot welding. Metals 2016;6(5):101.
[16] Li X, Liu F, Gong N, Yang C, Wang B. Surface topography induced high injection joining strength of polymer-metal composite and fracture mechanism. Compos Struct 2018;184:545–53.
[17] Li X, Xu D, Gong N, Xu Z, Wang L, Dong W. Improving the strength of injection molded aluminum/polyphenylene sulfide lap joints dependence on surface microstructure and composition. Mater Des 2019;179:107875.
[18] Meng X, Huang Y, Xie Y, Li J, Guan M, Wan L, et al. Friction self-riveting welding between polymer matrix composites and metals. Compos Part A Appl Sci Manuf 2019;127:105624.
[19] Altmeyer J, dos Santos JF, Amancio-Filho ST. Effect of the friction riveting process parameters on the joint formation and performance of Ti alloy/short-fibre reinforced polyether ether ketone joints. Mater Des 2014;60:164–76.
[20] Blaga L, Bancilă R, dos Santos JF, Amancio-Filho ST. Friction Riveting of glass–-fibre-reinforced polyetherimide composite and titanium grade 2 hybrid joints. Mater Des 2013;50:825–9.
[21] Liu FC, Dong P, Lu W, Sun K. On formation of Al O C bonds at aluminum/polyamide joint interface. Appl Surf Sci 2019;466:202–9.
[22] Lambiase F, Genna S, Kant R. A procedure for calibration and validation of FE modelling of laser-assisted metal to polymer direct joining. Opt Laser Technol 2018;98:363–72.
[23] Lambiase F, Genna S. Homogenization of temperature distribution at metal-polymer interface during Laser Direct joining. Opt Laser Technol 2020;128:106226.
[24] Lambiase F, Paoletti A, Grossi V, Genna S. Improving energy efficiency in friction assisted joining of metals and polymers. J Mater Process Technol 2017;250:379–89.
[25] Lambiase F, Paoletti A, Grossi V, Di Ilio A. Friction assisted joining of aluminum and PVC sheets. J Manuf Process 2017;29:221–31.
[26] Lambiase F, Paoletti A. Friction assisted joining of titanium and polyetheretherketone (PEEK) sheets. Thin-walled Struct 2018;130:254–61.
[27] Lambiase F, Paoletti A. Mechanical behavior of AA5053/polyetheretherketone (PEEK) made by friction assisted joining. Compos Struct 2018;189:70–8.
[28] Chen G-q, Shi Q-y, Li Y-j, Sun Y-j, Dai Q-l, Jia J-y, et al. Computational fluid dynamics studies on heat generation during friction stir welding of aluminum alloy. Comput Mater Sci 2013;79:540–6.
[29] Dialami N, Cervera M, Chiumenti M, Agelet de Saracibar C. A fast and accurate two-stage strategy to evaluate the effect of the pin tool profile on metal flow, torque and forces in friction stir welding. Int J Mech Sci 2017;122:215–27.
[30] Tutunchilar S, Haghpanahi M, Besharati Givi MK, Asadi P, Bahemmat P. Simulation of material flow in friction stir processing of a cast Al–Si alloy. Mater Des 2012;40:415–26.
[31] Veljic D, Perovic M, Sedmak A, Rakin M, Bajic N, Medjo B, et al. Numerical simulation of the plunge stage in friction stir welding. Struct Integr Life 2011;11(2):131–4.
[32] Malik V, Sanjeev NK, Hebbar HS, Kailas SV. Time efficient simulations of plunge and dwell phase of FSW and its significance in FSSW. Procedia Mater Sci 2014;5:630–9.
[33] Meyghani B, Awang MB, Poshteh RGM, Momeni M, Kakooei S, Hamdi Z. The effect of friction coefficient in thermal analysis of friction stir welding (FSW). IOP Conference Series: Materials Science and Engineering 495. 2019:012102.
[34] Essa ARS, Ahmed MMZ, Mohamed A-KYA, El-Nikhaily AE. An analytical model of heat generation for eccentric cylindrical pin in friction stir welding. J Mater Res Technol 2016;5(3):234–40.
[35] Schmidt H, Hattel J, Wert J. An analytical model for the heat generation in friction stir welding. Model Simul Mat Sci Eng 2004;12(1):143–57.
[36] Shi L, Wu CS. Transient model of heat transfer and material flow at different stages of friction stir welding process. J Manuf Process 2017;25:323–39.
[37] Zhang S, Chen G, Liu Q, Li H, Zhang G, Wang G, et al. Numerical analysis and analytical modeling of the spatial distribution of heat flux during friction stir welding. J Manuf Process 2018;33:245–55.
[38] Mykhaylyk VB, Burt M, Ursachi C, Wagner A. Thermal contact conductance of demountable in vacuum copper-copper joint between 14 and 100 K. Rev Sci Instrum 2012;83(3):034902.
[39] Numerical Simulation of Friction Welding Processes Based on ABAQUS Environment.
[40] Li W, Wang F, Shi S, Ma T. Numerical simulation of linear friction welding based on ABAQUS environment: challenges and perspectives. J Mater Eng Perform 2013;23(2):384–90.
[41] Brar NS, Joshi VS, Harris BW, Elert M, Furnish MD, Anderson WW, et al. Constitutive model constants for Al7075-T651 and Al7075-T6. 2009. p. 945–8.
[42] Bosco Jude S, Jinu GR, Arul Franco P. Comparision of experimental and simulated weld bead geometry by varying the weld speed in TIG welded AA7075 aluminium alloy. Mech Mech Eng 2016;20(8):377–92.